AGU PUBLICATIONS

Water Resources Research

RESEARCH ARTICLE
10.1002/2013WR014212

Key Points:
- An analytical solution for head in a sloping unconfined aquifer is developed
- The effect of the aquifer slope on temporal and spatial head is addressed
- The simplified free surface equation specified at the outcrop is assessed

Correspondence to:
H.-D. Yeh,
hdyeh@mail.nctu.edu.tw

Citation:
Huang, C.-S., S.-Y. Yang, and H.-D. Yeh (2014), Groundwater flow to a pumping well in a sloping fault zone unconfined aquifer, *Water Resour. Res.*, *50*, 4079–4094, doi:10.1002/2013WR014212.

Received 3 JUNE 2013
Accepted 30 APR 2014
Accepted article online 5 MAY 2014
Published online 20 MAY 2014

Groundwater flow to a pumping well in a sloping fault zone unconfined aquifer

Ching-Sheng Huang[1], Shaw-Yang Yang[2], and Hund-Der Yeh[1]

[1]Institute of Environmental Engineering, National Chiao Tung University, Hsinchu, Taiwan, [2]Department of Civil Engineering, Vanung University, Chungli, Taiwan

Abstract This study develops a mathematical model for simulating the hydraulic head distribution in response to pumping in a sloping fault zone aquifer under a water table boundary condition. A two-dimensional equation with a sink term representing the pumping is used for describing the head distribution in the aquifer. In addition, a first-order free surface equation is adopted to represent the change in water table at the outcrop. The analytical solution of the model, derived by the Laplace and finite Fourier cosine transforms, is expressed in terms of a double series. A finite difference solution within a deformable grid framework is developed to assess the solution obtained by specifying the free surface equation at the outcrop. Based on the analytical solution, we have found that the model's prediction tends to overestimate drawdown in a late pumping period. The temporal head distribution is independent of the aquifer slope if the water table change is small, and exhibits a double-humped shape due to the effect of the free surface. The temporal drawdown predicted from the analytical solution is further compared with those measured from a pumping test conducted in northern Portugal.

1. Introduction

There are two primary types of sloping unconfined aquifers: one is an aquifer with the water table as the upper boundary and a sloping impervious bed at the bottom, while the other is a sloping fault zone aquifer with the water table at the outcrop. The former involves water table change when subject to rainfall recharge. *Chapuis* [2011] reviewed analytical solutions for the problem involving steady state groundwater seepage due to recharge. He assessed the validation of those solutions using a finite element solution considering both saturated and unsaturated flows. On the other hand, the second type of aquifer, also called a sloping fracture, represents an aquifer in a rock fracture or a fault that connects the atmosphere with the free surface at the outcrop. The permeability of the surrounding rock in that case is generally much lower than that of the aquifer.

Analytical solutions which may be applicable to the sloping fault zone aquifer are reviewed as follows. *Hantush* [1962] considered a wedge-shaped aquifer connected to an external reservoir, where the water level varies temporally. He presented an analytical solution describing hydraulic head in the aquifer and indicated that the wedge-shaped aquifer cannot be approximated by a uniform one. *Latinopoulos* [1985] considered a rectangular aquifer where each side can be subject to either the Dirichlet, no-flow, or Robin boundary condition. He developed analytical solutions describing hydraulic head in the aquifer with different combinations of the boundary conditions. *Pacheco* [2002] considered a sloping fault zone aquifer extending semi-infinitely from the free surface at the outcrop. He used *Cooper and Jacob* [1946] solution to describe drawdown in the aquifer before the drawdown cone reaches the free surface. Free surface movement is approximated as a known function of time [*Pacheco*, 2002, Equation (7), p. 119] once the drawdown cone reaches the free surface. Nevertheless, such an approximation neglects the effect of gravity drainage from the free surface decline.

This current paper develops a mathematical model for describing two-dimensional (2-D) groundwater flow induced by pumping in a sloping fault zone aquifer with the water table at the outcrop. A first-order free surface equation is employed to describe a water table decline. A sink term in the 2-D flow equation represents a constant pumping rate for a vertical well. The analytical solution of the model, expressed in terms of a double series, is developed by applying the Laplace transform and finite Fourier cosine transform. The finite difference solution of the model within a deformable grid framework is also developed for

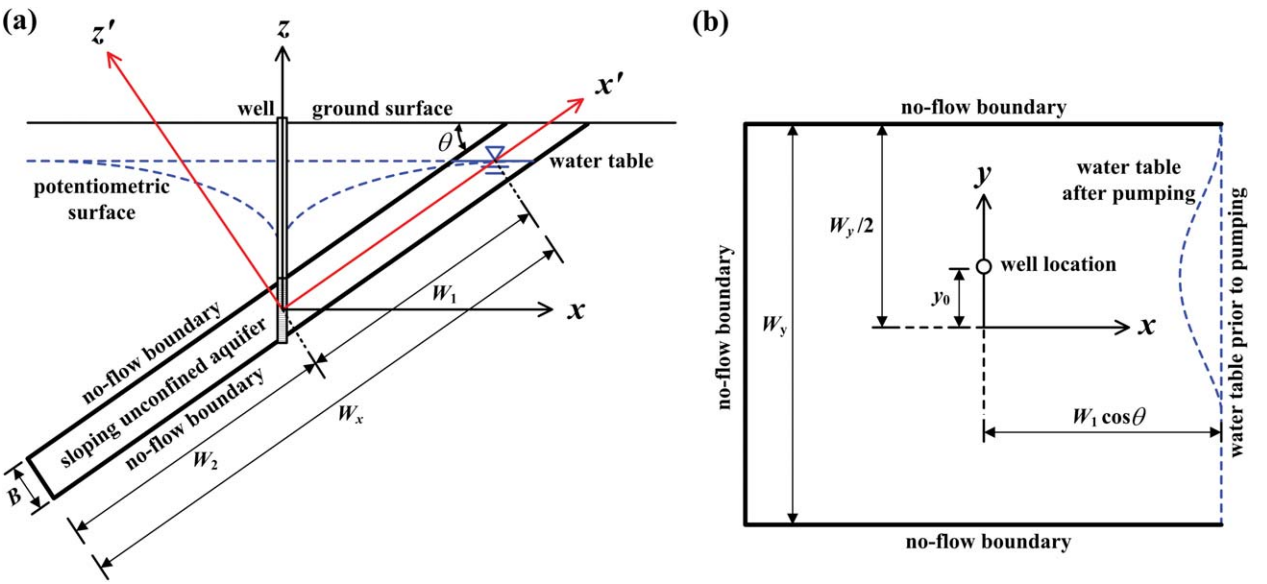

Figure 1. Schematic diagram of a sloping fault zone unconfined aquifer outcropping with the water table.

comparison with the analytical solution. The effect of the aquifer slope on temporal and spatial head distributions is investigated. Additionally, the temporal drawdown predicted by the analytical solution is compared with the field drawdown data observed in a pumping test by *Pacheco* [2002].

2. Mathematical Development

2.1. Conceptual Model

Rocks surrounding a sloping fault zone unconfined aquifer are regarded as an impermeable stratum when the ratio of the rock's hydraulic conductivity to that of the aquifer is less than 10^{-9} [*Huang et al*., 2012]. Figure 1 illustrates the schematic diagram of such a sloping fault zone unconfined aquifer with a pumping well. This aquifer extends finitely from the ground, outcrops with a free surface, slants with an angle θ, and has a thickness B as shown in Figure 1a. The x and y axes are horizontal, and the z axis is vertical in the Cartesian coordinate system. The x' and z' axes are parallel and perpendicular to the aquifer, respectively, in the sloping coordinate system. The well position is $(0, y_0)$ as shown in Figure 1b. The aquifer has finite W_x and W_y in width in the x'-direction and y-direction, respectively. The distance between the well and the free surface is W_1 in the x'-direction and $W_1 \cos\theta$ in the x-direction.

Consider 2-D groundwater flow in the sloping aquifer. The flow equation describing transient hydraulic head $h(x, y, t)$ in response to constant pumping can be expressed as

$$T\frac{\partial^2 h}{\partial x'^2}+T\frac{\partial^2 h}{\partial y^2}=S\frac{\partial h}{\partial t}+Q\delta\left(x'\right)\delta(y-y_0) \tag{1}$$

where T is the aquifer transmissivity, S is the aquifer storage coefficient, Q is a pumping rate, and $\delta()$ is the Dirac delta function. Equation (1) is applicable to 2-D flow in the sloping aquifer except in the case that the aquifer is horizontal or vertical. The case of the horizontal aquifer is trivial. For the vertical aquifer, one may refer to *Anderson* [2006].

The Dirac delta functions in equation (1) represent an infinitesimal well radius with negligible effects of a finite well radius and wellbore storage on the head. *Papadopulos and Cooper* [1967] mentioned that those effects greatly diminish when $t > 2.5\times10^2 r_c^2/T$, where r_c is the inner radius of a well. In addition, *Yeh and*

Chang [2013] also stated that the effects are negligible for a small-diameter well with a finite radius varying between 0.05 and 0.25 m.

The flow is static prior to pumping, and the hydraulic head is uniform over the whole domain. With the reference datum chosen at the free surface, the initial condition is therefore expressed as

$$h=0 \text{ at } t=0 \tag{2}$$

That is, the atmospheric pressure is set to zero. Based on equation (2), the hydraulic head h is negative for pumping, and its absolute value represents drawdown.

The first-order free surface equation describing vertical water table movement induced by pumping is written as

$$K\frac{\partial h}{\partial z}=-S_y\frac{\partial h}{\partial t} \text{ at } z=W_1\sin\theta+h \text{ and } x_o \le x \le x_f \tag{3}$$

where $K=T/B$ is the aquifer hydraulic conductivity, S_y is the specific yield, $x_o=W_1\cos\theta-B/(2\sin\theta)$, and $x_f=W_1\cos\theta+B/(2\sin\theta)$. Introduce the relation between the Cartesian and sloping coordinate systems as

$$\begin{aligned} x' &= x\cos\theta+z\sin\theta \\ y' &= y \\ z' &= -x\sin\theta+z\cos\theta \end{aligned} \tag{4}$$

Based on equation (4), equation (3) can be written as

$$K\left(\frac{\partial h}{\partial x'}\frac{\partial x'}{\partial z}+\frac{\partial h}{\partial z'}\frac{\partial z'}{\partial z}\right)=-S_y\frac{\partial h}{\partial t} \tag{5}$$

where $\partial x'/\partial z=\sin\theta$. The derivative term $\partial h/\partial z'$ approaches zero since the groundwater moves along the x'-direction. Under this condition, equation (5) reduces to

$$K\sin\theta\frac{\partial h}{\partial x'}=-S_y\frac{\partial h}{\partial t} \text{ at } x'=W_1+h/\sin\theta \tag{6}$$

Note that $W_1+h/\sin\theta$ represents a water table position in x'-direction and makes equation (6) nonlinear due to the presence of the unknown water table position. Equation (6) can be linearized by neglecting the last term $h/\sin\theta$ as

$$K\sin\theta\frac{\partial h}{\partial x'}=-S_y\frac{\partial h}{\partial t} \text{ at } x'=W_1 \tag{7}$$

which implies that the boundary condition is fixed at $x'=W_1$. This treatment is similar to the one taken by *Neuman* [1972] in developing an analytical solution for a horizontal unconfined aquifer.

The edges of the aquifer are considered under the no-flow condition as

$$\partial h/\partial x'=0 \text{ at } x'=-W_2 \tag{8}$$

$$\partial h/\partial y=0 \text{ at } y=\pm W_y/2 \tag{9}$$

where W_2 is the distance between the well and the bottom edge shown in Figure 1a. The beginning time accounting for the boundary effect on the head can be estimated by $R^2S/(16T)$ where R represents a shortest distance measured from the well to the boundaries of the aquifer [*Wang and Yeh*, 2008, Table II]. In

addition, each series of the model's solution, equations (14) and (15), converges faster when setting smaller widths of W_x and W_y.

Define dimensionless variables and parameters below

$$h_D=\frac{Th}{Q},\quad t_D=\frac{Tt}{SW_1{}^2},\quad x'_D=\frac{x'}{W_1},\quad x_D=\frac{x}{W_1},\quad y_D=\frac{y}{W_1},\quad y_{0D}=\frac{y_0}{W_1},$$
$$\sigma=\frac{S_yB}{SW_1\sin\theta},\quad \tau=\frac{Q}{TW_1\sin\theta}\quad \chi=\frac{W_2}{W_1},\quad \alpha=\frac{W_x}{W_1},\quad \xi=\frac{W_y}{W_1} \tag{10}$$

where the subscript D is used to denote the dimensionless variables. Based on equation (10), equations (1) and (2) and (6)–(9) can be written, respectively, as

$$\frac{\partial^2 h_D}{\partial x'^2_D}+\frac{\partial^2 h_D}{\partial y_D^2}=\frac{\partial h_D}{\partial t_D}+\delta\left(x'_D\right)\delta(y_D-y_{0D}) \tag{11}$$

$$h_D=0 \text{ at } t_D=0 \tag{11a}$$

$$\frac{\partial h_D}{\partial x'_D}=-\sigma\frac{\partial h_D}{\partial t_D} \text{ at } x'_D=1+\tau h_D \tag{11b}$$

$$\frac{\partial h_D}{\partial x'_D}=-\sigma\frac{\partial h_D}{\partial t_D} \text{ at } x'_D=1 \tag{11c}$$

$$\partial h_D/\partial x'_D=0 \text{ at } x'_D=-\chi \tag{11d}$$

$$\partial h_D/\partial y_D=0 \text{ at } y_D=\pm\xi/2 \tag{11e}$$

2.2. Analytical Solution

Applying the finite Fourier cosine transform to y_D and the Laplace transform to t_D in equations (11) and (11a) and (11c)-11e) results in an ordinary differential equation (ODE) in terms of x'_D. Solving the ODE simultaneously with the transformed boundary conditions yields the head solution in the Laplace and Fourier domain as

$$\overline{\overline{h}}_{D1}(x'_D,w_m,p)=\varphi(\chi,1-x'_D) \text{ for } 0\le x'_D\le 1 \tag{12}$$

$$\overline{\overline{h}}_{D2}(x'_D,w_m,p)=\varphi(\chi+x'_D,1) \text{ for } -\chi\le x'_D\le 0 \tag{13}$$

with

$$\varphi(a,b)=-\frac{\cosh(a\lambda)[\lambda\cosh(b\lambda)+\sigma p\sinh(b\lambda)]}{p\lambda[\sigma p\cosh(\alpha\lambda)+\lambda\sinh(\alpha\lambda)]}\cos\left[w_m\left(y_{0D}+\frac{\xi}{2}\right)\right] \tag{13a}$$

$$\lambda=\sqrt{w_m^2+p/\vartheta} \tag{13b}$$

$$w_m=\pi m/\xi \tag{13c}$$

where p is the Laplace transform parameter, and $m\in 1, 2, \ldots\infty$ is the finite Fourier cosine transform parameter. A detailed derivation of equations (12) and (13) is given in Appendix A. Application of complex analysis to the inverse Laplace transform leads to the head solution in the Fourier domain illustrated in Appendix B. Introducing the formula, equation (A3), for the inverse finite Fourier cosine transform to the Fourier-domain solution yields the head solution as

$$h_{D1}(x'_D,y_D,t_D)=\Phi(\chi,1-x'_D) \text{ for } 0\le x'_D\le 1 \tag{14}$$

$$h_{D2}(x'_D, y_D, t_D) = \Phi(\chi + x'_D, 1) \text{ for } -\chi \le x'_D \le 0 \tag{15}$$

with

$$\Phi(a,b) = \frac{1}{\xi}\left\{\begin{array}{c}\varphi_t(a,b) + \sum_{n=1}^{\infty}\varphi_n(a,b,0) + 2\sum_{m=1}^{\infty}[\varphi_s(a,b,w_m) + \varphi_0(a,b,w_m)]Y(m) \\ +2\sum_{m=1}^{\infty}\sum_{n=1}^{\infty}\varphi_n(a,b,w_m)Y(m)\end{array}\right\} \tag{15a}$$

$$\varphi_t(a,b) = -[3\mu_1(a^2+b^2) + 6\mu_1(t_D+\sigma b) - \mu_3]/(6\mu_1^2) \tag{15b}$$

$$\varphi_s(a,b,w) = -\cosh(aw)\cosh(bw)/[\vartheta w \sinh(\alpha w)] \tag{15c}$$

$$\varphi_0(a,b,w) = 2\cosh(a\beta_0)\exp[-\lambda_0(w)t_D][\beta_0\cosh(b\beta_0) - \sigma\lambda_0(w)\sinh(b\beta_0)]/\eta_0(w) \tag{15d}$$

$$\varphi_n(a,b,w) = 2\cos(a\beta_n)\exp[-\lambda_n(w)t_D][\beta_n\cos(b\beta_n) - \sigma\lambda_n(w)\sin(b\beta_n)]/\eta_n(w) \tag{15e}$$

$$Y(m) = \cos[\pi m(0.5 + y_D/\xi)]\cos[\pi m(0.5 + y_{0D}/\xi)] \tag{15f}$$

$$\eta_0(w) = \lambda_0(w)\{\mu_2\beta_0\cosh(\alpha\beta_0) + [1 - \sigma\alpha\lambda_0(w)]\sinh(\alpha\beta_0)\} \tag{15g}$$

$$\eta_n(w) = \lambda_n(w)\{\mu_2\beta_n\cos(\alpha\beta_n) + [1 - \sigma\alpha\lambda_n(w)]\sin(\alpha\beta_n)\} \tag{15h}$$

$$\lambda_0(w) = w^2 - \beta_0^2;\ \lambda_n(w) = w^2 + \beta_n^2 \tag{15i}$$

$$\mu_1 = \alpha + \sigma,\ \mu_2 = \alpha + 2\sigma,\ \mu_3 = \alpha^2(\alpha + 3\sigma) \tag{15j}$$

where w_m is defined in equation (13c) and β_0 and β_n are the roots of equations denoted, respectively, as

$$\exp(2\alpha\beta_0) = \frac{-\sigma\beta_0^2 + \beta_0 + \sigma w_m^2}{\sigma\beta_0^2 + \beta_0 - \sigma w_m^2} \tag{16}$$

and

$$\tan(\alpha\beta_n) = -\sigma(\beta_n^2 + w_m^2)/\beta_n \tag{17}$$

Notice that equation (16) has only one positive root, whereas equation (17) has infinite positive roots caused by the periodic function of $\tan(\alpha\beta_n)$. Estimates for β_0 and β_n are given in section 2.3. The solution, equations (14) and (15), is composed of four terms. The first term is the closed form expression for ϕ_t; the second and third terms contain the simple series expanded in terms of β_n and m, respectively; the last term is the double series expanded in terms of m and β_n. Equation (15b) is a first-order polynomial in time, indicating that there is no steady state head distribution.

The water table position can be approximated as

$$x'_{Dapprox.} = 1 + \tau h_{D1} \tag{18}$$

where h_{D1}, a function of y_D and t_D, is the head predicted from equation (14) with $x'_D = 1$. The absolute value of h_{D1} represents drawdown. The term $h_{D1}/\sin\theta$ reflects water table movement along the negative direction of x'_D-axis. Thus, the problem domain falls in the range of $x'_D \le x'_{Dapprox.}$. The $x'_{Dapprox.}$ will be compared with $1 + \tau h_D$ where h_D is predicted by the finite difference solution developed based on equation (11b) in section 2.4. This comparison will be illustrated in section 3.3.

2.3. Calculation of β_0 and β_n

The roots in equations (16) and (17), β_0 and β_n, can be found by Newton's method with appropriate initial guess values. The roots are the intersection points of the left-hand side (LHS) and right-hand side (RHS) functions of equation (16) for β_0 and (17) for β_n. The root β_0 is very close to the vertical asymptote of the

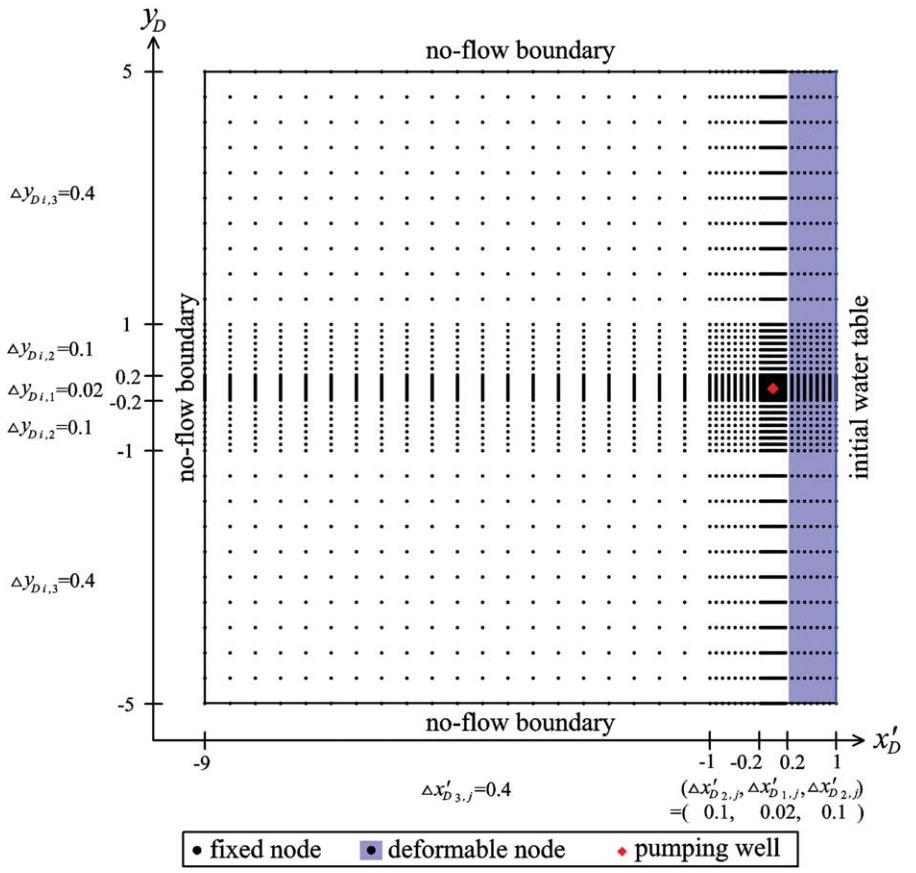

Figure 2. Schematic diagram of nodal points for the finite difference solution.

RHS function of equation (16). The initial guess for β_0 is chosen as the position of the asymptote derived by setting the denominator of the RHS function to zero, and in turn expressed as

$$\beta_{0initial}=\delta+(-1+\sqrt{1+4(\sigma w_m)^2})/(2\sigma) \tag{19}$$

where δ is a small positive value, say $\delta=10^{-8}$, to prevent the denominator from being zero in the iteration process. Similarly, the roots β_n are also close to the vertical asymptotes of the LHS function, tan $(\alpha\beta_n)$. The initial guesses for β_n are therefore chosen as

$$\beta_{ninitial}=\delta+(2n-1)\pi/(2\alpha) \tag{20}$$

where $n \in 1, 2, \ldots\infty$.

2.4. Finite Difference Solution

An implicit finite difference method is applied to approximate equations (11)–(11b) and (11d) and (11e) for comparison with the present analytical solution developed based on equation (11c). A nonuniform finite difference grid is used to discretize the problem domain, and its nodal points are shown in Figure 2. Assume that the aquifer has a dimensionless width of 10 in the x'_D-direction and y_D-direction, and the problem domain falls in the range of $-9 \le x'_D \le 1$ and $-5 \le y_D \le 5$. The pumping well is located at the origin ($x'_D=0$ and $y_D=0$). The region near the well has small grid sizes and away from the well has large grid sizes.

Equation (11) is approximated as

$$\frac{h_{D_{i+1,j}}^{n+1}-2h_{D_{i,j}}^{n+1}+h_{D_{i-1,j}}^{n+1}}{(\Delta x'_{Dk,j})^2}+\frac{h_{D_{i,j+1}}^{n+1}-2h_{D_{i,j}}^{n+1}+h_{D_{i,j-1}}^{n+1}}{(\Delta y_{Di,k})^2} = \frac{h_{D_{i,j}}^{n+1}-h_{D_{i,j}}^{n}}{\Delta t_D}+\begin{cases}[(\Delta x'_{D1,j})(\Delta y_{Di,1})]^{-1} & \text{at well position}\\ 0 & \text{else where}\end{cases} \tag{21}$$

where Δt_D is a dimensionless time step, $t_D=\Delta t_D\times n$ is the present time, $h_{D_{i,j}}^{n+1}$ is the hydraulic head at nodal point (i, j), and time t_D, $h_{D_{i,j}}^{n}$ is the head at one step earlier than $h_{D_{i,j}}^{n+1}$, and $k \in 1, 2$, and 3. The integer pair (i, j) is ordered from the LHS boundary in the x'_D-direction and from the lower boundary in the y_D-direction. The grid sizes $\Delta x'_{D1,j}$, $\Delta x'_{D2,j}$, and $\Delta x'_{D3,j}$ in the x'_D-direction are 0.02 for $-0.2 \le x'_D \le 0.2$, 0.1 for $-1 \le x'_D \le -0.2$ and $0.2 \le x'_D \le 1$, and 0.4 for $-9 \le x'_D \le -1$, respectively, as shown in Figure 2. Similarly, the grid sizes $\Delta y_{Di,1}$, $\Delta y_{Di,2}$, and $\Delta y_{Di,3}$ in y_D-direction are 0.02 for $-0.2 \le y_D \le 0.2$, 0.1 for $-1 \le y_D \le -0.2$ and $0.2 \le y_D \le 1$, and 0.4 for $-5 \le y_D \le -1$ and $1 \le y_D \le 5$, respectively.

The initial condition of equation (11a) can be denoted as

$$h_{D_{i,j}}^{1}=0 \text{ at each } (i,j) \tag{22}$$

Equation (11d) representing the no-flow boundary at the first i is approximated as

$$h_{D_{i-1,j}}^{n+1}=h_{D_{i+1,j}}^{n+1} \text{ at } i=1 \tag{23}$$

Similarly, equation (11e) representing the no-flow boundaries for the first and last j is approximated, respectively, as

$$h_{D_{i,j-1}}^{n+1}=h_{D_{i,j+1}}^{n+1} \text{ at } j=1 \tag{24}$$

$$h_{D_{i,j-1}}^{n+1}=h_{D_{i,j+1}}^{n+1} \text{ at } j=n_y \tag{25}$$

where n_y denotes the total number of nodes in y_D-direction, and $(0, j)$, $(i, 0)$, and (i, n_y+1) are the positions of fictitious nodes outside the no-flow boundaries.

Consider a deformable grid framework in the region of $0.2 \le x'_D \le 1$ as shown in Figure 2, where water table movement is described by equation (11b). In this region, the grid size remains constant before the movement. The grid sizes $\Delta y_{Di,1}$, $\Delta y_{Di,2}$, and $\Delta y_{Di,3}$ remain constant while the grid size $\Delta x'_{D2,j}$ decreases to match a new location of the water table. The deformable grid size $\Delta x'^{n+1}_{D_j}$ is then adjusted according to the water table location at the previous time step as

$$\Delta x'^{n+1}_{D_j}=\frac{W_d+\tau h_{D_{i,j}}^{n}}{n_d} \text{ at } i=n_x \tag{26}$$

where n_x is the total number of the grids in x'_D-direction, W_d (the region width) is 0.8, and n_d (the number of the grids inside the region) is 8. Note that the grid size $\Delta x'^{n+1}_{D_j}$ will be changed at each time step, and the n_x and n_d maintain constant during the entire simulation time. Equation (11b), which describes the water table movement, can be approximated as

$$\frac{h_{D_{i,j}}^{n+1}-h_{D_{i-1,j}}^{n+1}}{\Delta x'^{n+1}_{D_j}}=-\sigma\frac{h_{D_{i,j}}^{n+1}-h_{D_{i,j}}^{n}}{\Delta t_D} \text{ at } i=n_x \tag{27}$$

where $\Delta x'^{n+1}_{D_j}$ has been defined by equation (26). In the numerical simulation, the time increment Δt_D is set to 1, and the simulation period is $0 \le t_D \le 1460$ (365 day).

Table 1. Default Values to Variables and Hydraulic Parameters

		Field Data (unit)		
Notation	Default Value (unit)	E3	E5	Description
h	none	none	none	Hydraulic head
(x', y, t)	(−50 m, 0, 0.01 day)	(0.07m, 0, 280 min)	(0.07m, 0, 110 min)	Variables of sloping Cartesian coordinate, and time variable
y_0	0	0	0	Well position in y-direction
B	30 m	35 m	35 m	Aquifer thickness in z'-direction
T	30 m^2/d	1.2×10^{-3} m^2/min	3.5×10^{-4} m^2/min	Transmissivity
S	3×10^{-3}	6.1×10^{-4}	6.1×10^{-4}	Storage coefficient
Q	100 m^3/d	0.0342 m^3/min	0.0354 m^3/min	Pumping rate
K	1 m/d	3.4×10^{-5} m/min	1.0×10^{-5} m/min	Hydraulic conductivity defined as $K = T/B$
(S_y, θ)	(0.2, π/6)	(0.01, π/4)	(0.01, π/4)	Aquifer specific yield and slope, respectively
(W_1, W_2)	(50 m, 450 m)	(178 m, 322 m)	(184 m, 316 m)	Distance measured from the well to the top and bottom boundaries, respectively, in x'-direction
(W_x, W_y)	(500 m, 500 m)	(500 m, 500 m)	(500 m, 500 m)	Aquifer widths in x'-direction and y-direction, respectively, and $W_x = W_1 + W_2$
(h_{D1}, h_{D2})	none	none	none	Th/Q for $0 \le x'_D \le 1$ and $-\chi \le x'_D \le 0$, respectively
(x'_D, y_D, t_D)	(−1, 0, 0.04)	(3.9×10^{-4}, 0, 0.017)	(3.8×10^{-4}, 0, 1.9×10^{-3})	$(x'/W_1, y/W_1, Tt/(SW_1^2))$
y_{0D}	0	0	0	y_0/W_1
(σ, τ)	(80, 0.133)	(4.56, 0.226)	(4.41, 0.777)	$(S_y B/(SW_1 \sin\theta), Q/(TW_1 \sin\theta))$
(χ, α, ξ)	(9, 10, 10)	(1.81, 2.81, 2.81)	(1.72, 2.72, 2.71)	$(W_2/W_1, W_x/W_1, W_y/W_1)$

3. Results and Discussion

This section analyzes hydraulic head predicted by the analytical solution and the finite difference solution. In section 3.1, the influence of the aquifer slope on temporal and spatial head distributions is assessed. In section 3.2, the effects of the no-flow and water table boundaries on a temporal head distribution is investigated. In section 3.3, the use of equation (11c) to develop the analytical solution is evaluated and discussed. In these three sections, default values of variables and hydraulic parameters are given in the second column of Table 1. In section 3.4, the application of the present solution to a real-world case is presented.

3.1. Effect of Aquifer Slope on Head

The aquifer slope affects late parts of a temporal head distribution. Figure 3 illustrates the temporal distributions of hydraulic head $h_{D2}(-0.2, 0, t_D)$ and $h_{D2}(-1, 0, t_D)$ predicted by equation (15) when $\theta = 20°$, 45°, and 60°. The hydraulic head $h_{D1}(1, 0, t_D)$ predicted by equation (14) is also considered, and its absolute value $|h_{D1}|$ is used to approximate a water table decline as illustrated in Figure 3. When $t_D < 6$, there is no difference in predicted head h_{D2} for various θ. When $t_D \ge 6$, the water table represented by $|h_{D1}|$ declines significantly, and a larger θ leads to a smaller head h_{D2} at a specific time. It seems reasonable to conclude that the change in the aquifer slope does not affect the temporal head distributions before the occurrence of a significant water table decline.

Figure 4 shows the spatial head distribution predicted by equation (14) for $\theta = 0$, 20°, 45°, and 60°. We consider $t_D = 0.04$ for avoiding the boundary effect. The *Theis* [1935] solution for a horizontal confined aquifer is taken for comparison. The figure indicates that the spatial head distributions plotted in the horizontal coordinate system for varied θ are different. The reason for difference from them is because the varying value of θ causes different x'_D by the relationship $x'_D = x_D/\cos\theta$ for a fixed x_D. Accordingly, the *Theis* [1935] solution for a horizontal confined aquifer can be used to account for the slope effect prior to the boundary effect when replacing the radial variable r by $r/\cos\theta$. The *Theis* [1935] solution gives the same predicted result as the present analytical solution for each θ.

3.2. Boundary Effect on Temporal Head

The free surface, described by equation (11c), causes temporally varied flow in a double-humped shape, which exhibits unconfined behavior. Figure 5 demonstrates the temporal head distributions of $h_{D1}(1, 0, t_D)$ predicted by equation (14) and $h_{D2}(-1, 0, t_D)$ predicted by equation (15) for $\sigma = 40$ ($S_y = 0.1$) and 80 ($S_y = 0.2$). The absolute value of the head $|h_{D1}|$ denotes a vertical water table decline, as illustrated in Figure 5. That figure shows that the temporal head distribution of h_{D2} reaches its flat stage in the period of $4 \le t_D \le 10$, when σ=40 or $4 \le t_D \le 20$ when σ=80. The flat stage is due to gravity drainage at x'_D=1, and

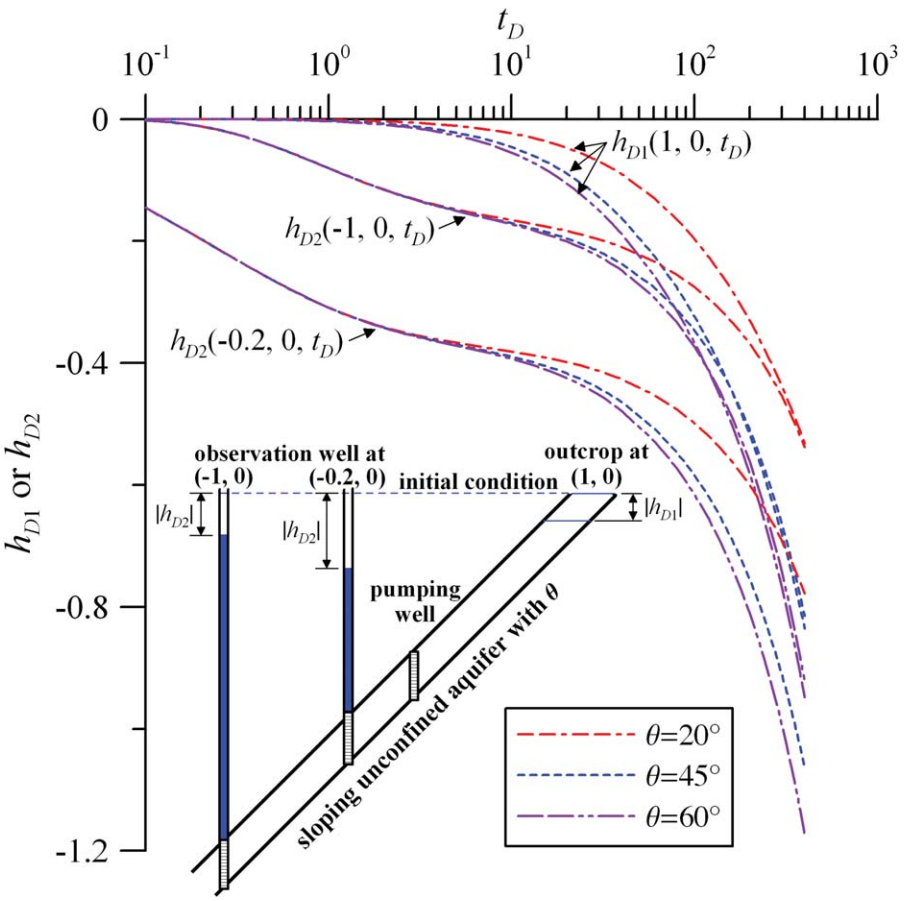

Figure 3. Temporal distributions of hydraulic head at the observation wells of (−1, 0) and (−0.2, 0) and at the outcrop of (1, 0) predicted by the analytical solution for various aquifer slopes.

a larger σ leads to a longer flat stage. The flat stage occurs at $t_D = 4$, with a significant water table decline represented by $|h_{D1}|$. On the other hand, the no-flow boundary at the edges of the aquifer makes the temporal head distribution decrease dramatically. Figure 6 shows the temporal distributions of $h_{D2}(-1, 0, t_D)$ for the aquifer widths of $\alpha = \xi = 10$ (500 m) and 20 (1000 m). Both curves deviate at $t_D = 20$, indicating the boundary effect on the head distribution in the case of $\alpha = \xi = 10$. Note that the effect of the no-flow boundary is more apparent at the later period than that of the water table boundary because the pumping well is closer to the outcrop, as shown in Figure 6.

3.3. Free Surface Equation

The finite difference solution is used to assess a water table decline predicted based on equation (11c), which is commonly used to develop analytical solutions [e.g., *Neuman*, 1972; *Zhan and Zlotnik*, 2002; *Huang et al*., 2012]. Figure 7 illustrates the spatial head distributions predicted by the analytical solution and finite difference solution at times of 4 (1 day), 400 (100 day), and 1460 (365 day). The numerical solution considers the free surface boundary, described by equation (11b) specified at the dynamic water table. On the other hand, the analytical solution is developed based on the free surface equation fixed at the outcrop (i.e., $x'_D = 1$). Consequently, the location of the water table can be approximated by equation (18). The water table declines predicted by both solutions are along the aquifer slope, as shown in the figure. When $t_D = 4$, the predicted head distributions from both solutions agree well and are near symmetrical to the well because of the insignificant water table decline at $x_D = 0.86$. The figure however indicates that the analytical solution overestimates the drawdown at the late pumping times of $t_D = 400$ and 1460. Furthermore, the temporal head distributions at the locations of (−6.6, 0) and (−3, 0) and at the outcrop of (1, 0) predicted by both solutions are drawn in Figure 8. The results predicted by the analytical solution are valid before

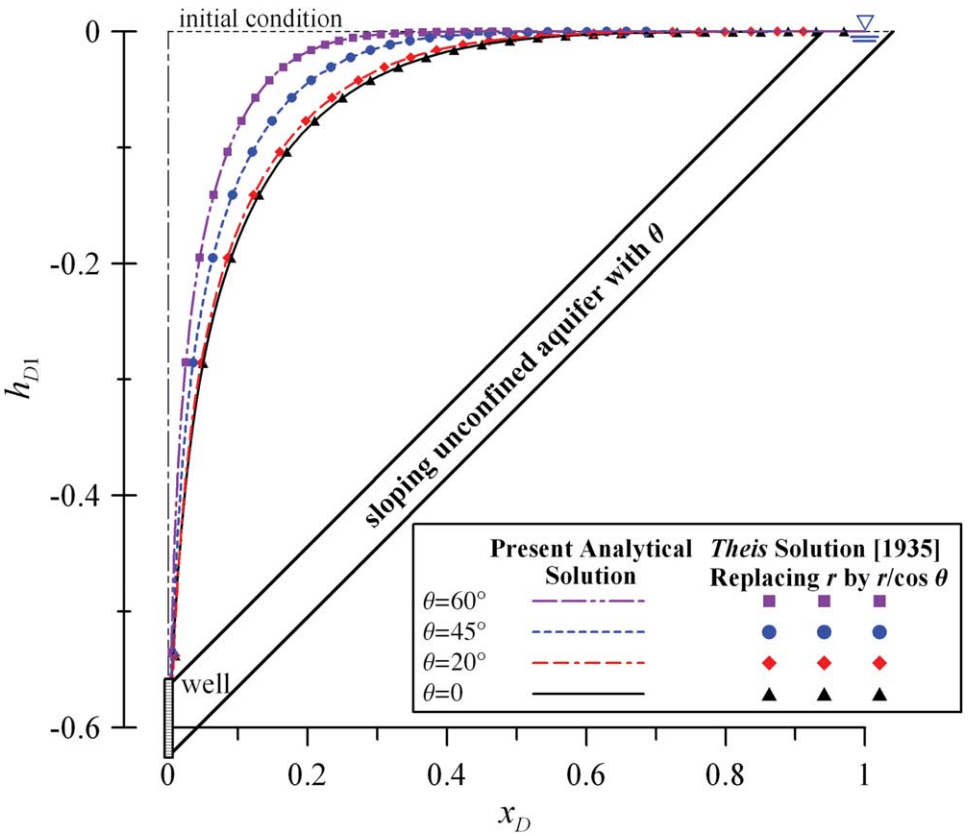

Figure 4. Spatial distributions of hydraulic head at $y_D = 0$ predicted by the analytical solution and the *Theis* [1935] solution for various aquifer slopes when $t_D = 0.04$.

$t_D = 10$ that is 2.5 day calculated based on $t=(SW_1^2)t_D/T$ for the values of T, S, and W_1 (=50 m) given in Table 1. After $t_D = 10$, the analytical solution underestimates the hydraulic head (or overestimates the drawdown) because of the simplification of equation (11b) to (11c) by specifying the free surface equation at the outcrop (i.e., $x'_D=1$). However, the location to specify this equation should follow the water table, which moves toward the well as time increases. In engineering practice, a large distance between a pumping well and the outcrop should be seriously considered for much groundwater exploitation. Accordingly, the analytical solution can give fairly good prediction before $t = 100$ day for the given default values except that $W_1 = 320$ m.

3.4. Comparison With Field Data

Pacheco [2002] reported a pumping test conducted in a geologic formation consisting mostly of serpentine rocks splitting with several fractures in the study region. Crushed materials with clay minerals fill these fractures. The fractures distribute anomalously and crisscross with each other. Eleven pumping wells were installed and named as serial numbers from E1 to E11. One fracture with E3 and E5 wells corresponds with the present model considering a single fracture with a pumping well [*Pacheco*, 2002, FZ3 in Figure 5, p. 124]. The pumping rates at E3 and E5 wells are 0.0342 and 0.0354 m^3/min, respectively. The radius for both wells is 0.07 m. The drawdown data observed from E3 and E5 wells are shown in Figure 9a. The fracture inclines approximately 45° toward the southwest, and its average thickness is 35 m. A schematic diagram of the fracture with the wells is shown in Figure 9b.

Pacheco [2002] indicated that the values of T and S range from 8.4×10^{-5} to 1.2×10^{-2} m^2/min and from 2×10^{-5} to 6.1×10^{-2}, respectively. Accounting for the aquifer heterogeneity, the values of T are chosen as 1.2×10^{-3} and 3.5×10^{-4} m^2/min, and the values of K are 3.4×10^{-5} and 1.0×10^{-5} m/min for the local aquifer near E3 and E5 wells, respectively. The S is set as 6.1×10^{-4} and S_y is set as 0.01 because of the presence of the clay formation. The hydraulic parameters mentioned above are shown in Table 1.

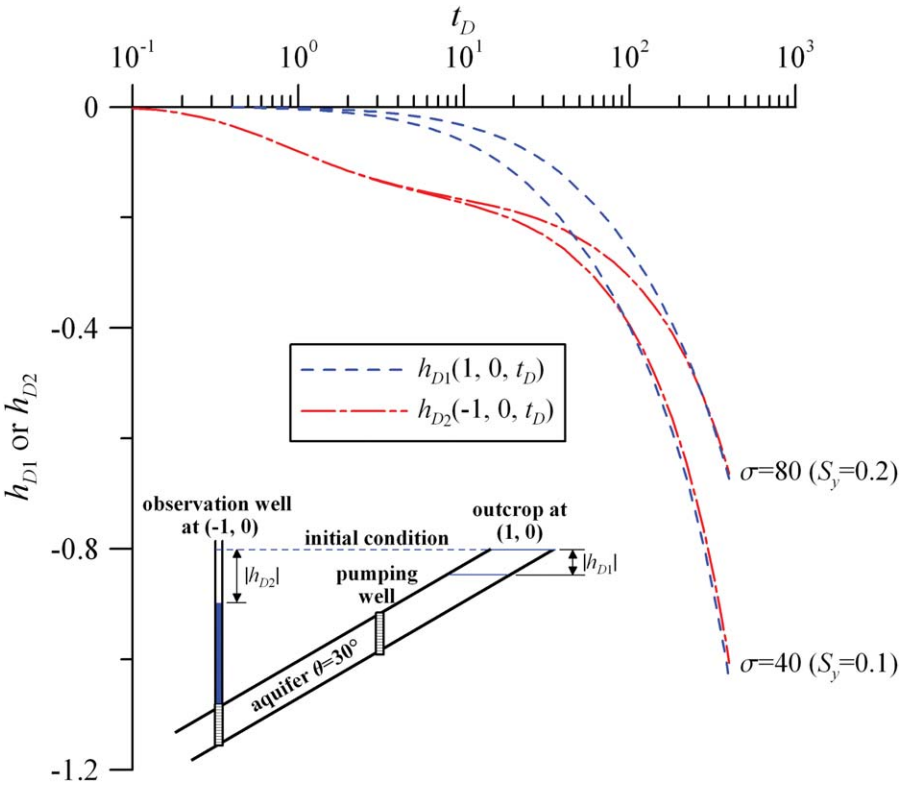

Figure 5. Temporal distributions of hydraulic head at the observation well of (−1, 0) and at the outcrop of (1, 0), as predicted by the analytical solution for different specific yields.

The time-drawdown curves predicted by equation (14) are compared with those predicted by the *Pacheco* [2002] solution and the field data observed at E3 and E5 wells [*Pacheco*, 2002] shown in Figure 9a. The E3 and E5 wells operated for 280 and 110 min, respectively. The drawdown cones induced by E3 and E5 wells have not reached the outcrop at $t = 280$ and 110 min, respectively, as illustrated in Figure 9b, implying that the flow is still under the confined condition. Figure 9a reveals that both solutions overestimate the drawdown over the whole pumping period. This discrepancy may be attributed to water recharge from adjacent small fractures and a nearby fault zone [*Pacheco*, 2002, FZ4 in Figure 5, p. 124] mentioned in *Pacheco and Van der Weijden* [2012]. In addition, the difference in the predicted drawdown curves is mainly because the Pacheco solution is developed based on the Cooper-Jacob formula.

4. Concluding Remarks

A mathematical model has been developed for simulating groundwater flow due to pumping in a sloping fault zone unconfined aquifer outcropping with a free surface. A 2-D equation with a sink term representing a pumping well is used for describing the flow in the sloping aquifer. A first-order free surface equation specified at the outcrop describes water table movement while the no-flow boundary is imposed for the other edges of the aquifer. The analytical solution of the model, derived by the Laplace transform and finite Fourier cosine transform, is expressed as a double series expanded in terms of integers as well as roots β_0 and β_n. The roots are determined by Newton's method with the initial guesses represented by analytical expressions. Furthermore, the finite difference solution of the model is developed within a deformable grid framework to simulate the position of the dynamic water table at the outcrop. Additionally, the drawdown distribution predicted by the analytical solution is compared with field data observed from a pumping test reported in *Pacheco* [2002]. Main conclusions providing new physical insights can be drawn below:

1. The aquifer slope does not affect a temporal head distribution before a significant water table decline taking place.

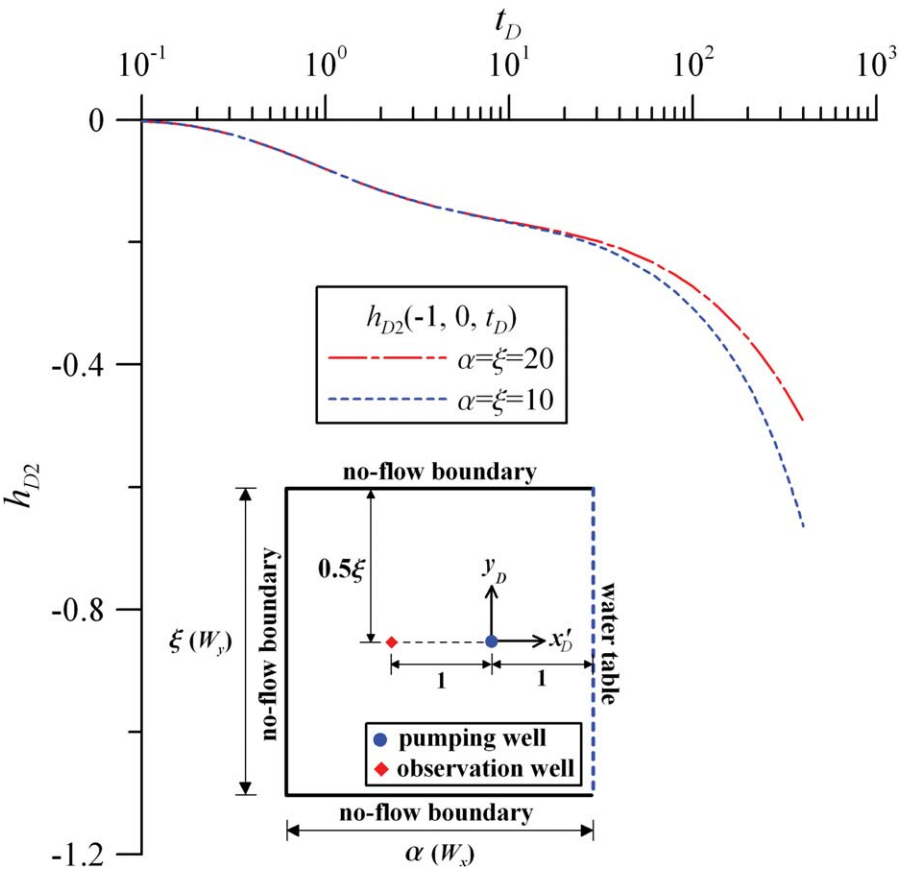

Figure 6. Temporal distributions of hydraulic head at the observation well of (−1, 0) predicted by the analytical solution for different aquifer widths.

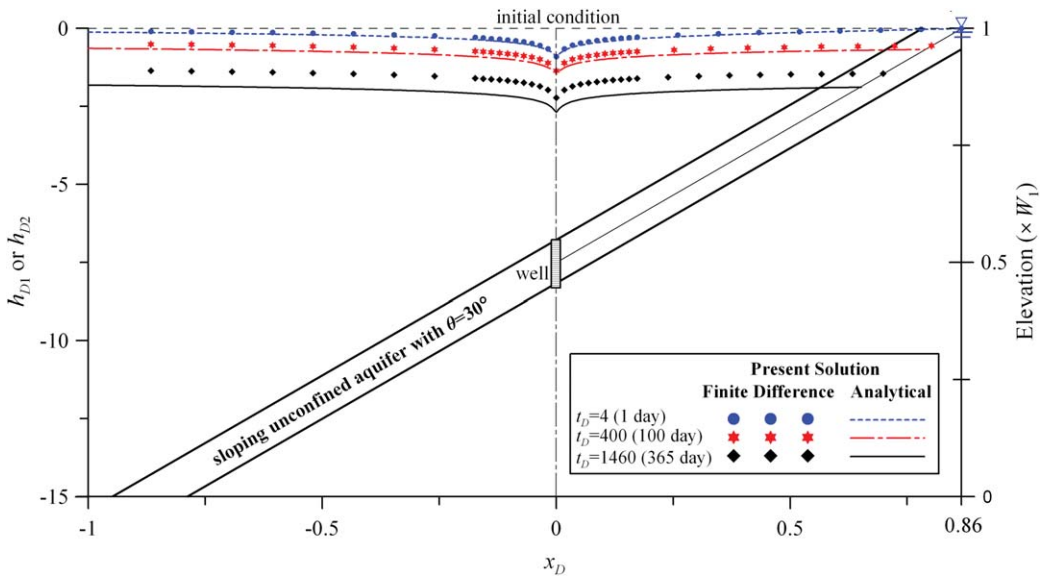

Figure 7. Spatial distributions of hydraulic head at $y_D = 0$ predicted by the analytical solution and finite difference solution for different times.

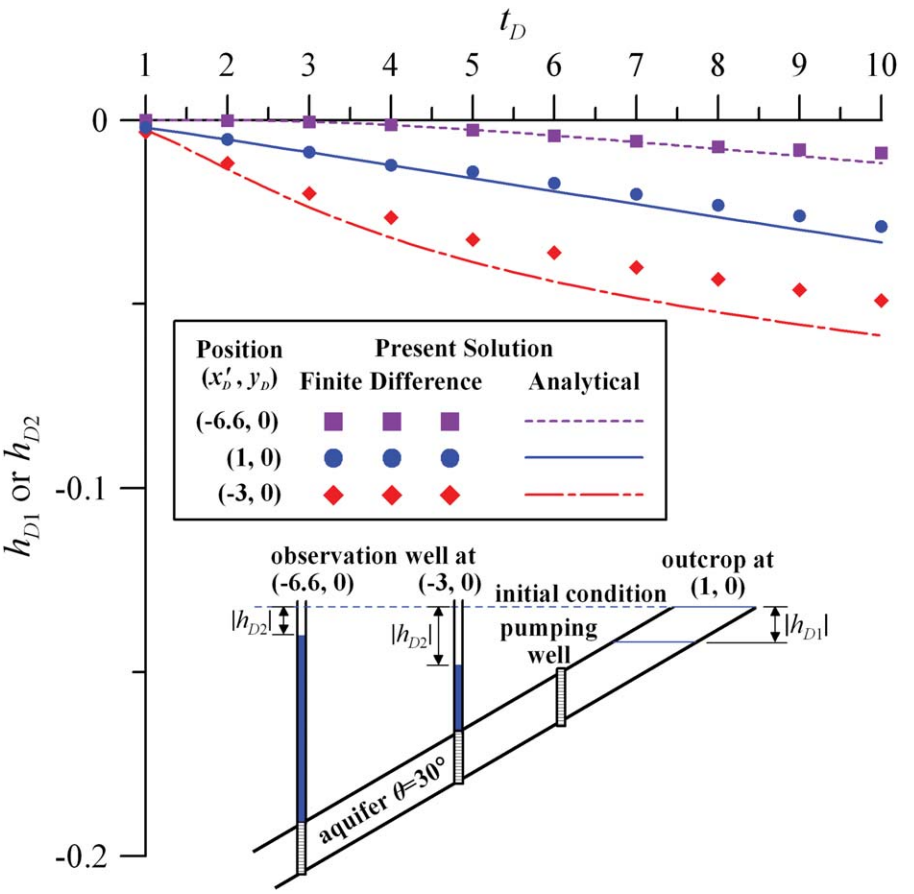

Figure 8. Temporal distributions of hydraulic head at the observation wells of (−6.6, 0) and (−3, 0) and at the outcrop of (1, 0) predicted by the analytical solution and finite difference solution.

2. The spatial head distribution in the horizontal coordinate system depends on the aquifer slope because of the relationship of $x'_D = x_D/\cos\theta$.

3. The *Theis* [1935] solution, replacing r by $r/\cos\theta$, is applicable to evaluating the effect of the slope on a spatial head distribution before a significant water table decline taking place.

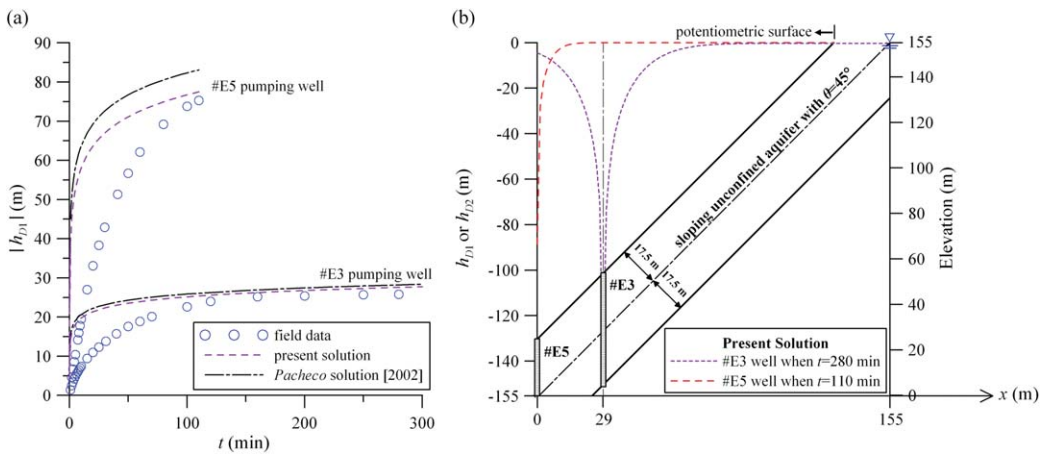

Figure 9. Comparison of the temporal drawdown distributions predicted by the analytical solution and *Pacheco* [2002] solution with the field drawdown data reported by *Pacheco* [2002].

4. The time-drawdown curve for a sloping fault zone unconfined aquifer exhibits a double-humped shape due to gravity drainage once the water table declines.

5. The predicted head distribution obtained based on the assumption that the free surface equation is fixed at the outcrop is valid for a short dimensionless pumping period and tends to overestimate drawdown for a long one.

Appendix A: Derivation of Equations (12) and (13)

The definition of the finite Fourier cosine transform is expressed as

$$\bar{h}_D(m)=\int_{-\xi/2}^{\xi/2} h_D \cos\left[w_m\left(y_D+\frac{\xi}{2}\right)\right]dy_D \tag{A1}$$

where w_m is defined by equation (13c). The transform has the property of

$$\int_0^{\xi}\frac{\partial^2 h_D}{\partial y_D^2}\cos\left(w_m y_D\right)dy_D=(-1)^m\frac{\partial h_D}{\partial y_D}\Big|_{y_D=\xi/2}-\frac{\partial h_D}{\partial y_D}\Big|_{y_D=-\xi/2}-w_m^2\bar{h}_D(m) \tag{A2}$$

The first and second RHS terms equal zero due to equation (11e). The formula for the inverse finite Fourier cosine transform can be written as

$$h_D=\frac{1}{\xi}\bar{h}_D(0)+\frac{2}{\xi}\sum_{m=1}^{\infty}\bar{h}_D(m)\cos\left[w_m\left(y_D+\frac{\xi}{2}\right)\right] \tag{A3}$$

On the other hand, the definition of the Laplace transform is expressed as

$$\bar{\bar{h}}_D(p)=\int_0^{\infty}\bar{h}_D\exp\left(-pt_D\right)dt_D \tag{A4}$$

It has the property of

$$\int_0^{\infty}\frac{\partial\bar{h}_D}{\partial t_D}\exp\left(-pt_D\right)dt_D=p\bar{\bar{h}}_D-\bar{h}_D|_{t_D=0} \tag{A5}$$

where $\bar{h}_D$ is the head transformed by the finite Fourier cosine transform. The second RHS term equals zero because of equation (11a).

After applying these two transforms to equations (11), (11a), and (11c)-11e), the resultant ODE and transformed boundary conditions in terms of x'_D are rewritten as

$$\frac{\partial^2\bar{\bar{h}}_D}{\partial x'^2_D}-\left(p+w_m^2\right)\bar{\bar{h}}_D=\frac{1}{p}\cos\left[w_m\left(y_{0D}+\frac{\xi}{2}\right)\right]\delta\left(x'_D\right) \tag{A6}$$

$$\frac{\partial^2\bar{\bar{h}}_D}{\partial x'_D}=-\sigma p\bar{\bar{h}}_D \text{ at } x'_D=1 \tag{A7}$$

$$\partial\bar{\bar{h}}_D/\partial x'_D=0 \text{ at } x'_D=-\chi \tag{A8}$$

where p is the Laplace transform parameter. Equation (A6) can be separated according to the Dirac delta function $\delta\left(x'_D\right)$ into two homogeneous ODEs as

$$\frac{\partial^2 \bar{\bar{h}}_D}{\partial x'^2_D} - (p + w_m^2)\bar{\bar{h}}_{D1} = 0 \text{ for } 0 \le x'_D \le 1 \tag{A9}$$

$$\frac{\partial^2 \bar{\bar{h}}_D}{\partial x'^2_D} - (p + w_m^2)\bar{\bar{h}}_{D2} = 0 \text{ for } -\chi \le x'_D \le 0 \tag{A10}$$

Two requirements at $x'_D = 0$ are needed to solve the ODEs. One is the continuity of the transformed hydraulic head denoted as

$$\bar{\bar{h}}_{D1} = \bar{\bar{h}}_{D2} \text{ at } x'_D = 0 \tag{A11}$$

The other can be obtained by integrating equation (A6) to x'_D from $x'_D = 0^-$ to $x'_D = 0^+$ as

$$\frac{\partial^2 \bar{\bar{h}}_{D1}}{\partial x'_D} - \frac{\partial^2 \bar{\bar{h}}_{D2}}{\partial x'_D} = \frac{1}{p}\cos\left[w_m\left(y_{0D} + \frac{\xi}{2}\right)\right] \text{ at } x'_D = 0 \tag{A12}$$

which reflects the discontinuity of the flux at $x'_D = 0$ due to $\delta(x'_D)$. Note that the integration of the second LHS term in equation (A6) equals zero because of equation (A11). Solving equations (A9) and (A10) simultaneously with equations (A7), (A8), (A11), and (A12) leads to equations (12) and (13).

Appendix B: Inverse Laplace Transform of Equation (13a)

The function ϕ defined by equation (13a) is a single-value function of p in a complex plane. The single-value function gives the only result to a specific p and has no branch cut that reflects spatial discontinuity between p^+ and p^-. Therefore, $\varphi(p^+)$ equals $\varphi(p^-)$ for any complex number p. One can confirm $\varphi(p^+) = \varphi(p^-)$ in the following way. Let p^+ and p^- be in terms of the polar coordinate with the origin at $p = -w_m^2$ obtained from the root of $\lambda(p) = 0$ as

$$p^+ = r\exp(i\delta) - w_m^2 \tag{B1}$$

$$p^- = r\exp[i(\delta - 2\pi)] - w_m^2 \tag{B2}$$

where r is a radius from the origin, δ is an argument between 0 and 2π, and i is the imaginary unit. Note that equations (B1) and (B(2)) have the same result in terms of a complex number. Substituting equations (B1) and (B2) into equation (13b), respectively, yields

$$\lambda = \sqrt{r}\exp(i\delta/2) = \sqrt{r}[\cos(\delta/2) + i\sin(\delta/2)] \tag{B3}$$

$$\lambda = \sqrt{r}\exp[i(\delta - 2\pi)/2] = -\sqrt{r}[\cos(\delta/2) + i\sin(\delta/2)] \tag{B4}$$

Notably, equations (B3) and (B4) differ in the negative sign. The results of substituting equations (B3) and (B4) separately into equation (13a) are the same, indicating $\varphi(p^+) = \varphi(p^-)$ and no branch cut.

Since ϕ is a single-value function, an integral contour for its inverse Laplace transform consists of a straight line and a semicircle. The straight line extends from $p = r - i\infty$ to $p = r + i\infty$ where r herein represents a positive value to contain all of the poles of the function ϕ. The semicircle has an infinite radius and connects the straight line to enclose those poles. The integral along the semicircle is zero because of the infinite radius. According to the residue theory, the time domain inversion equals the sum of the residues of the inside poles. Each residue can be estimated by the following formula

$$Res = \frac{1}{(m-1)!}\lim_{p \to \wp}\left\{\frac{d^{m-1}}{dp^{m-1}}[\varphi(p) \times (p - \wp)^m]\right\} \tag{B5}$$

where $\wp$ represents the location of the pole of the function ϕ, and m is the order of the pole.

The locations of the poles are determined by setting the denominator of equation (13a) to be zero as

$$p\lambda[\sigma p\cosh(\alpha\lambda)+\lambda\sinh(\alpha\lambda)]=0 \quad \text{(B6)}$$

where $\lambda=\sqrt{w_m^2+p}$. The roots of the equation represent the locations of the poles in a complex plane and appear only at the negative part of the real axis. Note that $p=-w_m^2$ derived from $\lambda=0$ is not a pole because the power of $\sqrt{w_m^2+p}$ is 1/2 rather than an integer. Equation (B6) will be analyzed according to the value of w_m.

When $w_m > 0$, equation (B6) obviously has one simple pole at $p = 0$. According to equation (B5), the residue equals the product of $\cos[w_m(y_{0D}+\xi/2)]$ and ϕ_s defined by equation (15c). In addition, other poles can be obtained numerically by

$$\sigma p\ \cosh(\alpha\lambda)+\lambda\ \sinh(\alpha\lambda)=0 \quad \text{(B7)}$$

which is derived from setting the term in the bracket of equation (B6) to be zero. One simple pole is located at $p = p_0$ between $p = 0$ and $p=-w_m^2$. Let $\lambda=\sqrt{w_m^2+p_0}=\beta_0$ for conciseness, and thus one obtains $p_0=\beta_0^2-w_m^2$. Substituting $\lambda=\beta_0$ and $p=p_0$ into equation (B7) and rearranging the result yields equation (16). With the value of β_0, the location of the simple pole can be obtained by $p_0=\beta_0^2-w_m^2$. Its residue is derived by applying equation (B5) as the product of $\cos[w_m(y_{0D}+\xi/2)]$ and ϕ_0 defined by equation (15d). On the other hand, behind $p=-w_m^2$, there are infinite simple poles at $p=p_n$ where $n \in 1, 2, 3, \ldots\infty$. For preventing the residues of these poles from the imagery unit i, we let $\lambda=\sqrt{w_m^2+p_n}=i\beta_n$ and have $p_n=-\beta_n^2-w_m^2$. Substituting $\lambda=i\beta_n$ and $p=p_n$ into equation (B7) and rearranging the result leads to equation (17). With the values of β_n, the locations of those simple poles can be estimated by $p_n=-\beta_n^2-w_m^2$. The residues are expressed by applying equation (B5) as the product of $\cos[w_m(y_{0D}+\xi/2)]$ and ϕ_n defined by equation (15e).

When $w_m=0$, equation (B6) reduces to

$$p^2[\sigma\lambda\cosh(\alpha\lambda)+\sinh(\alpha\lambda)]=0 \quad \text{(B8)}$$

where $\lambda=\sqrt{p}$. Apparently, one second-order pole is at $p = 0$. Applying equation (B5) results in its residue as ϕ_t defined by equation (15b). Furthermore, infinite simple poles are at $p = p_n$ behind $p = 0$. The residues can be obtained directly by substituting $w_m = 0$ into equation (15e).

Acknowledgments
The authors are very much grateful to the esteemed reviewers for their valuable comments and suggestions. Research leading to this paper has been partially supported by the grants from Taiwan National Science Council under the contract NSC 101-2221-E-009-105-MY2 and NSC 102-2221-E-009-072-MY2.

References

Anderson, E. I. (2006), Analytical solutions for flow to a well through a fault, *Adv. Water Resour.*, *29*(12), 1790–1803, doi:10.1016/j.advwatres.2005.12.010.

Chapuis, R. P. (2011), Steady state groundwater seepage in sloping unconfined aquifers, *Bull. Eng. Geol. Environ.*, *70*(1), 89–99, doi:10.1007/s10064-010-0282-2.

Cooper, H. H., and C. E. Jacob (1946), A generalized graphical method for evaluating the formation constants and summarizing well field history, *Trans. AGU*, *27*, 526–534.

Hantush, M. S. (1962), Flow of ground water in sands of nonuniform thickness Part 1. Flow in a wedge-shaped aquifer, *J. Geophys. Res.*, *67*(2), 703–709.

Huang, C.-S., H.-D. Yeh, and C.-H. Chang (2012), A general analytical solution for groundwater fluctuations due to dual tide in long but narrow islands, *Water Resour. Res.*, *48*, W05508, doi:10.1029/2011WR011211.

Latinopoulos, P. (1985), Analytical solutions for periodic well recharge in rectangular aquifers with third-kind boundary conditions, *J. Hydrol.*, *77*, 293–306.

Neuman, S. P. (1972), Theory of flow in unconfined aquifers considering delayed response of the water table, *Water Resour. Res.*, *8*(4), 1031–1045.

Pacheco, F. A. L. (2002), Response to pumping of wells in sloping fault zone aquifers, *J. Hydrol.*, *259*(1-4), 116–135, doi:10.1016/S0022-1694(01)00584-4.

Pacheco, F. A. L., and C. H. Van der Weijden (2012), Weathering of plagioclase across variable flow and solute transport regimes, *J. Hydrol.*, *420-421*, 46–58, doi:10.1016/j.jhydrol.2011.11.044.

Papadopulos, I. S., and H. H. Cooper (1967), Drawdown in a well of large diameter, *Water Resour. Res.*, *3*(1), 241–244.

Theis, C. V. (1935), The relation between the lowering of the piezometric surface and the rate and duration of discharge of a well using ground-water storage, *Trans. AGU*, *16*, 519–524.

Wang, C. T., and H. D. Yeh (2008), Obtaining the steady-state drawdown solutions of constant-head and constant-flux tests, *Hydrol. Processes*, *22*, 3456–3461, doi:10.1002/hyp.6950.

Yeh, H. D., and Y. C. Chang (2013), Recent advances in modeling of well hydraulics, *Adv. Water Resour.*, *51*, 27–51, doi:10.1016/j.advwatres.2012.03.006.

Zhan, H., and V. A. Zlotnik (2002), Groundwater flow to a horizontal or slanted well in an unconfined aquifer, *Water Resour. Res.*, *38*(7), 1108, doi:10.1029/2001WR000401.